Navier-Stokes Analyses of the Redistribution of Inlet Temperature Distortions in a Turbine

Man Mohan Rai*
NASA Ames Research Center, Moffett Field, California
and
Robert P. Dring†
United Technologies Research Center, East Hartford, Connecticut

The flow exiting the combustor and entering the turbine of a gas turbine engine is known to contain both spatial and temporal variations in total temperature. Although historically it has been presumed that the turbine rotor responds to the average temperature, recent experimental evidence has demonstrated that the rotor actually separates the hotter and cooler streams of fluid so that the hotter fluid migrates toward the pressure surface and cooler fluid migrates toward the suction surface. In the present study a time-accurate, two-dimensional, thin-layer, Navier-Stokes analysis of a turbine stage is used to analyze this phenomenon. The rough qualitative agreement between the measured and the computed results indicates that the analysis has successfully captured many of the important features of the flow.

Nomenclature

C_p = pressure coefficient
C_T = temperature coefficient
$\bar{C}_T$ = temperature fluctuation coefficient
c = local speed of sound
M = Mach number
p = pressure
p_t = total pressure
R_1, R_2, R_3 = Riemann invariants
T_{av} = area-averaged inlet temperature
T_{min}, T_{max} = minimum and maximum temperatures over a cycle, respectively
U = rotor velocity
u, v = Cartesian velocity components in the (x,y) directions, respectively
x, y = Cartesian physical coordinates
γ = ratio of specific heats
ρ = density

Introduction

THE exit flow from a gas turbine combustor entering a turbine stage can have wide variations in temperature. These variations may be both spatial and temporal. To achieve high cycle efficiencies the average combustor exit temperature must be high. This leads to peak turbine airfoil temperatures that exceed allowable metal temperatures by as much as 500-1000°F.[1] Several methods are used to keep the surface temperatures at tolerable values. These include augmenting internal-cooling passages and introducing cooling air into the hot stream so that the metal comes into contact with cooler air. Additional details regarding these and other methods can be found in Ref. 1. The implementation of these cooling methods requires a clear understanding of the aerodynamics involved. Both qualitative and quantitative assessments of the redistribution of inlet temperature distortions can be used to considerable advantage by the turbine designer.

Earlier work[2] showed theoretically that in the absence of inlet total pressure variations, inlet temperature variations will not change streamline patterns in stationary rows. However, this is not the case for the rotating blade rows. References 3 and 4 present secondary flow analyses indicating that inlet temperature nonuniformities can lead to secondary flows in the rotating rows. Reference 5 shows that a nonuniform, inflow total temperature leads to a segregation of hot and cold gases on the airfoils in question. A detailed discussion of earlier work can be found in Ref. 1.

Reference 1 presents experimental and analytical investigations of the temperature redistribution phenomena for an axial stage. A hot streak of air (twice the temperature of the rest of the inlet flow) seeded with carbon dioxide (CO_2) was introduced through a circular pipe at 40% span upstream of, and midway between, two stator airfoils. The total pressure within the hot streak was the same as that of the rest of the inlet fluid. Tests were conducted with both heated and unheated air exiting the circular pipe. The location of the seeded air was determined by measuring CO_2 concentrations at various locations within the stage. Results demonstrating the unaffected streamlines in the stator row (thus confirming the theoretical predictions of Ref. 2) are presented. Reference 1 also presents results showing the streamline patterns in the rotor row caused by secondary flows which in turn are caused by the inlet temperature distortion. The results indicate the migration of the hot gas to the pressure side of the rotor and the cooler gases to the suction side of the rotor. This leads to a local hot spot on the pressure side of the rotor. It was also found that more fluid from the hot streak reached the hub and tip end walls on the pressure side of the channel.

The temperature redistribution problem is an ideal candidate for computational fluid dynamics techniques. Both surface and passage temperatures (in addition to other fluid dynamic variables) are obtained as a part of the calculation. One does not have to resort to measuring auxiliary quantities such as CO_2 concentration to obtain an understanding of the temperature distribution or streamline patterns in the stage.

This study presents results obtained from a time-accurate, two-dimensional, thin-layer, Navier-Stokes calculation of the entire stage. The flow is inherently unsteady because of the

Presented as Paper 87-2146 at the AIAA/SAE/ASME/ASEE 23rd Joint Propulsion Conference, San Diego, CA, June 29-July 2, 1987; received Aug. 19, 1987; revision received March 9, 1989.

*Research Scientist. Associate Fellow AIAA.
†Manager, Gas Turbine Technology. Member AIAA.

relative motion of the rotor with respect to the stator. The computer program used to perform the stage calculation was developed in Ref. 6. Details regarding the program and the numerical methodology are presented in the next section. The current calculation accurately simulates interaction effects (such as unsteadiness) and viscous effects. Results include both time-averaged surface temperatures and the temporal variations of the surface temperature. The effects of inlet temperature distortions on the time-averaged surface pressures are also discussed. Contours depicting temporal- and spatial-temperature variations in the stator and rotor passages are included. A comparison of time-averaged temperatures with the experimental results of Ref. 1 is presented. In light of the fact that the purpose of this study was to explore the ability of the calculation to capture the dominant physics of a hot streak, no attempt was made to eliminate a number of differences between the experimental setup and the computation. These differences will be discussed.

Numerical Methodology

The time-dependent, thin-layer, Navier-Stokes equations in two spatial dimensions are solved using an iterative, implicit, upwind, finite-difference algorithm developed in Refs. 6 and 7. The method is second-order accurate in time and space. The flow is assumed to turbulent, and the eddy viscosity is calculated using the Baldwin-Lomax model.[8] The kinematic viscosity of the fluid is determined using Sutherland's law.

The airfoil geometry used is the same as that of Refs. 1 and 9 at midspan. Figure 1 shows the shape of the rotor and stator airfoils and their orientations relative to each other and the inlet flow direction. The stator and rotor rows consisted of 22 and 28 airfoils, respectively. A Navier-Stokes calculation with a total of 50 airfoils would be extremely time consuming. To overcome this difficulty, the rotor airfoils were enlarged by a factor of (28/22), keeping the pitch-to-chord ratio the same. It was then assumed (for the calculation) that there were only 22 airfoils in the rotor row. This assumption makes it possible to perform a calculation with only one rotor airfoil and one stator airfoil (a periodicity boundary condition is used to simulate the presence of the rest of the blades). The axial gap between them was chosen to be 15% of the average chord length, whereas the actual axial gap in Ref. 1 was 65% of the average chord length.

Solving the Navier-Stokes equations using the finite-difference method requires a discretization of the region of interest. Many fluid flow problems are defined over regions in space that can be discretized with a single finite-difference grid. However, the rotor-stator problem is geometrically complex, and it is difficult to discretize the corresponding region with a single grid. In this study we use a multiple-zone approach in which the region of interest is divided into several zones and grids are generated independently for each zone.

The grid system chosen for the calculation consists of four different zones. The first zone contains the stator airfoil and is discretized with an O grid. The second zone contains the rotor airfoil and is also discretized with an O gird. The grids in these zones were generated using an elliptic grid generator and are shown in Fig. 2. Although the actual grids used for the calculation are very dense near the airfoil surfaces (to resolve the viscous effects), for the purpose of clarity Fig. 2 shows grids in which the points are equispaced in the direction normal to the airfoil surfaces.

Zones 3 and 4 are shown in Fig. 3. The grids for these zones are generated algebraically. Zone 3 contains zone 1 and, consequently, the stator airfoil. Zones 1 and 3 are stationary with respect to each other. The relationship between zones 2 and 4 is similar to that between zones 1 and 3. Additionally, zones 3 and 4 abut on each other along the patch boundary ABCD (Fig. 3). These two zones (3 and 4) slip past each other as the rotor airfoil moves downward. Zones 3 and 4 constitute a patched-grid system. Figure 4 shows all of the grids used for the calculation.

The use of multiple grids in simulating the flow over the rotor-stator configuration (shown in Fig. 4) results in several

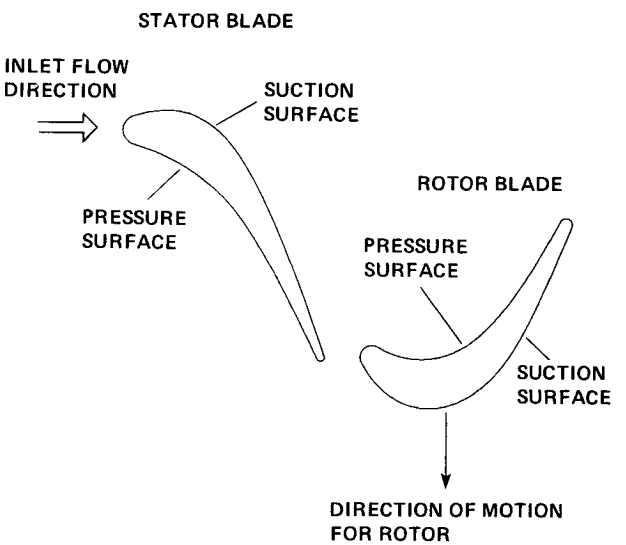

Fig. 1 Rotor-stator geometry.

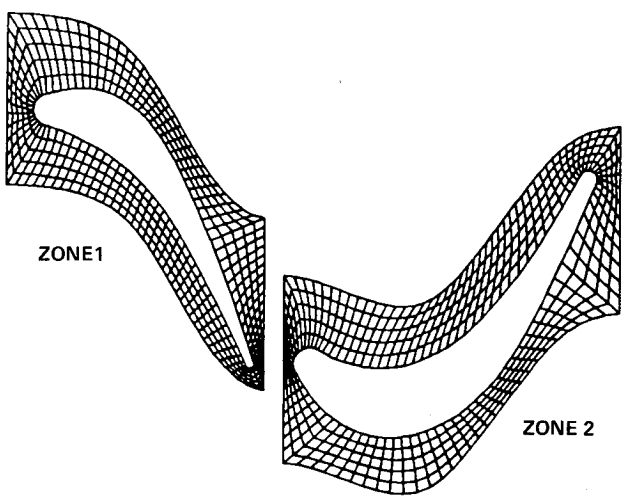

Fig. 2 O-type grids for zones 1 and 2.

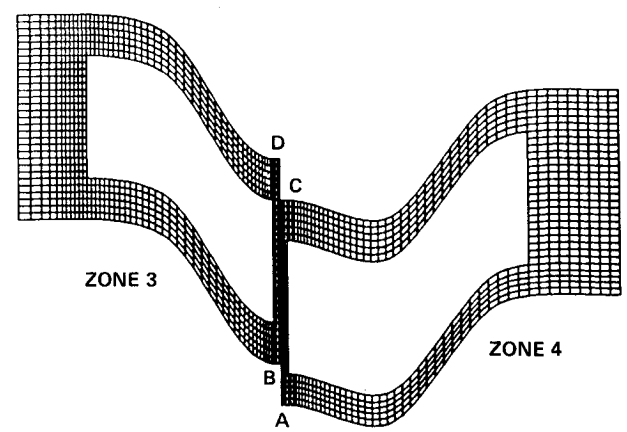

Fig. 3 Algebraically generated grids for zones 3 and 4.

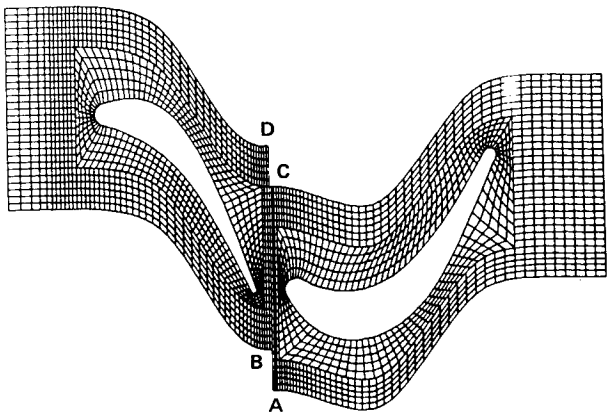

Fig. 4 Discretization of rotor-stator geometry.

computational boundaries. The boundary conditions used at each of these boundaries are briefly outlined next.

The inner boundaries of the two O grids correspond to the airfoil surfaces and, hence, the no-slip condition, and adiabatic wall conditions (or wall temperature) are imposed at these boundaries. It should be noted that in the case of the rotor airfoil, no-slip does not imply that the absolute velocity at the surface of the airfoil is zero, but rather that the relative velocity is zero. In addition to the no-slip condition, the derivative of pressure in the direction normal to the wall surface is set to zero.

The left boundary of zone 3 is a subsonic inlet boundary. Three quantities need to be specified at this boundary. The three chosen for this study are the Riemann invariants

$$R_1 = u + \frac{2c}{\gamma - 1} \tag{1a}$$

$$R_3 = \frac{p}{\rho^\gamma} \tag{1b}$$

and the inlet flow angle, which in this case is equivalent to

$$v_{\text{inlet}} = 0 \tag{2}$$

The dependent variables u, v, p, ρ, and c are specified so that the inlet flow contains a streak of high-temperature gas midway between the stator airfoils. The fourth quantity (which is necessary to update the points on this boundary) is also a Riemann invariant

$$R_2 = u - \frac{2c}{\gamma - 1} \tag{3}$$

and is extrapolated from the interior of zone 3. The manner in which these boundary conditions can be implemented implicitly is described in Ref. 10.

The calculation assumes that there are an infinite number of rotor and stator airfoils in the positive and negative y directions in Fig. 4. Hence, a simple periodicity boundary condition is imposed on the upper and lower boundaries of zones 3 and 4. The implicit implementation of this boundary condition is straightforward and will not be discussed here.

The right boundary of zone 4 is a subsonic exit boundary. A simple implicit extrapolation procedure is used at this boundary. The implicit extrapolation is followed by a postupdate correction in which the exit static pressure is specified. Prescribing the exit static pressure results in pressure waves being reflected back into the system. However, these reflections are not expected to distort the time-averaged temperatures or pressures for the configuration and flow conditions under consideration. The resultant distortion of the unsteady pressures is relatively minor and will be discussed in a future article.

The present calculation uses both patched grids (grids that come together along common lines) and overlaid grids (grids that have a common area of overlap). The region of overlay is not clear from Fig. 4. Although information from zone 3 is transferred to zone 1 at the patch boundary (clearly seen in Fig. 4), the information from zone 1 is transferred to zone 3 at the grid points of zone 3 that lie in zone 1. This is possible because the zone-3 grid exists under the zone-1 grids, although this overlap is not shown in Fig. 4 for the purpose of clarity. The boundary conditions used to transfer information from grid to grid are discussed in Ref. 6 and, in the interest of brevity, are not included here.

Results

In this section results are presented for the rotor-stator configuration shown in Fig. 4. These results were obtained by integrating the thin-layer Navier-Stokes equations using the integration method and the boundary conditions mentioned in the preceding section. The flowfield was initialized with freestream conditions everywhere, and the finite-difference equations were integrated until a periodic solution in time was obtained. Approximately five cycles (a cycle corresponds to the motion of the upper boundary of zone 4 from its current position to the position occupied currently by the lower boundary of zone 4) were required to get rid of the initial transients and establish a solution that was periodic in time. The last two cycles of the calculation were performed with 2000 integration steps per cycle.

The dependent variables were nondimensionalized with respect to the inlet pressure (p_∞) and density (ρ_∞). This yields

$$u_\infty = M_\infty \sqrt{\gamma} \tag{4a}$$

$$v_\infty = 0 \text{ (inlet flow is axial)} \tag{4b}$$

where M_∞ is the inlet Mach number. For the purpose of initializing the dependent variables in the four zones and also specifying the Riemann invariants R_1 and R_3, it was assumed that M_∞ was equal to 0.07. The rotor velocity was adjusted during the calculation so that the flow coefficient was 0.78 (defined as being equal to u_∞/U where U is the velocity of the rotor). The temperature in the hot streak was taken to be 1.2 times the rest of the inlet gas (which is at T_∞). The hot streak was assumed to exist over a quarter of the length of the inlet boundary, thus resulting in an average inlet temperature T_{av} equal to $1.05T_\infty$. The static and total pressure in the hot streak were assumed to be the same as the rest of the inlet flow. This results in the following identities:

$$\rho_{hs} = \rho_\infty / 1.2 \tag{5a}$$

$$u_{hs} = u_\infty \times \sqrt{1.2} \tag{5b}$$

$$v_{hs} = v_\infty \times \sqrt{1.2} \tag{5c}$$

$$M_{hs} = M_\infty \tag{5d}$$

where the subscript hs represents the hot streak. These conditions within the hot streak were imposed indirectly through the Riemann invariants as discussed in the preceding section.

The hot streak in the experiment (Ref. 1) was different from that used in the described analysis. Instead of having one hot streak per airfoil passage, as used in the analysis, the experiment had only one hot streak for the entire turbine. Thus, at any instant, only one of the 22 stator passages contained a hot streak. In addition, the total temperature of the hot streak in the experiment was twice that of the surrounding fluid; in the analysis this ratio was 1.2. The implications of these differences will be examined more thoroughly when the measured and computed results are compared.

Time-Averaged Pressure

Figure 5 shows the time-averaged pressure coefficient C_p as a function of the axial distance along the stator. The pressure coefficient is defined as

$$C_p = \frac{p_{avg} - (p_t)_{inlet}}{\frac{1}{2}\rho_{inlet}U^2}$$

where p_{avg} is the static pressure averaged over one cycle, $(p_t)_{inlet}$ is the average total pressure at the inlet, ρ_{inlet} is the average density at the inlet, and U is the velocity of the rotor airfoil. Figure 5 also shows the experimentally obtained pressure distribution of Ref. 9 (obtained without the hot streak). There is excellent agreement between theory and experiment. This proximity of the two sets of results should be expected because the hot streak is at the same static and total pressures as the rest of the inlet air and also does not impact the stator airfoils. A numerical calculation without the hot streak yielded stator surface pressures that were almost identical to those obtained with the hot streak. A small separation bubble was found on the trailing-edge circle of the stator in the numerical results. This is seen as a sharp dip and rise of C_p toward the trailing edge of the stator. The experimental data also indicate such a separation.

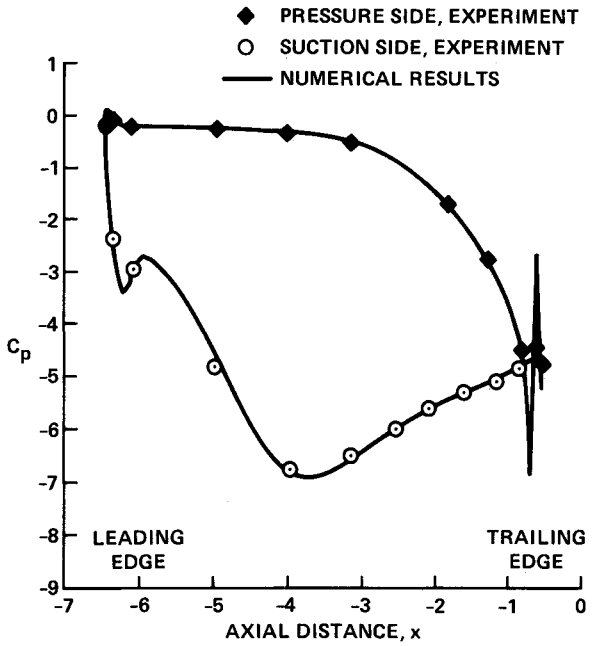

Fig. 5 Time-averaged pressure distribution on the stator.

Figure 6 shows the time-averaged C_p distribution for the rotor. The agreement between the numerical and experimental results is good, except on the suction side of the blade toward the trailing edge ($4.0 \leq x \leq 7.0$). This difference between the calculated and experimental results is because of the three-dimensionality of the real flow (the present calculation is two-dimensional in nature). The disappearance of this difference between theory and experiment with a three-dimensional calculation is documented in Ref. 11. There is a good match between the experimental and numerical results on the pressure side, thus indicating that the stator-exit-absolute flow angle was calculated accurately (causing the measured and calculated relative total pressures to be close to each other). A small separation bubble was found on the rotor trailing-edge circle, as it was in the case of the stator airfoil. The bubble is seen as a spatial fluctuation in pressure. Just as in the case of the stator, the rotor C_p values obtained numerically without the hot streak (not shown here) were once again almost identical to those obtained with the hot streak. This is surprising, considering that the rotor does come in contact with the hot streak during its travel, and the relative total pressure of the hot streak is higher than that of the cool surrounding fluid.

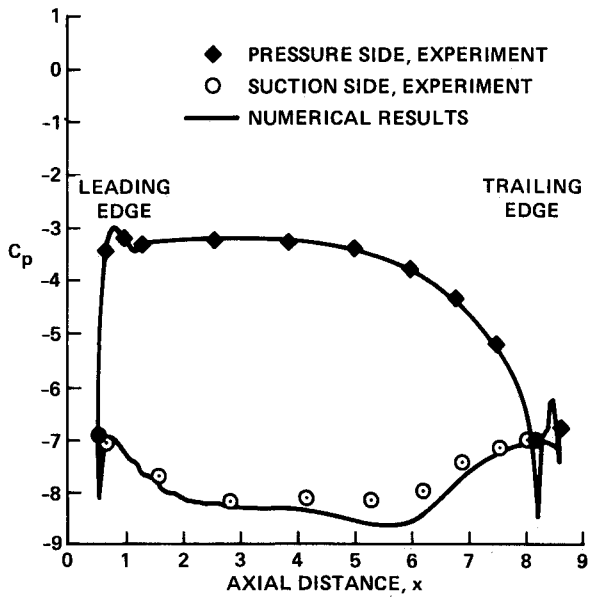

Fig. 6 Time-averaged pressure distribution on the rotor.

Time-Averaged Temperatures

The surface temperature of the stator is almost equal to the temperature of the unheated inlet gas (T_∞) on the entire stator surface. This is to be expected because the stator does not come into contact with the hot streak. The rotor, on the other hand, passes through a hot streak every cycle and, hence, the rotor surface temperatures are significantly altered.

Figure 7 shows the time-averaged, temperature-coefficient distribution (C_T) on the rotor. The temperature coefficient is defined as

$$C_T = \frac{T - T_\infty}{T_{av} - T_\infty}$$

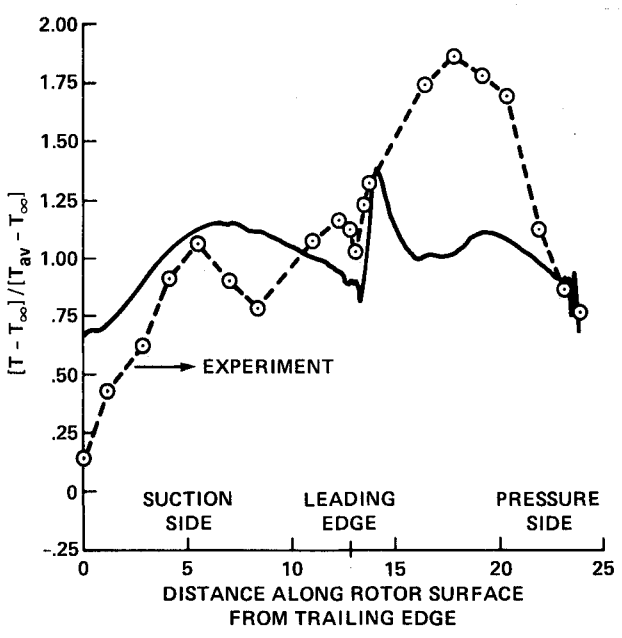

Fig. 7 Time-averaged temperature distribution on the rotor.

Since the rotor passes through the hot streak, rotor surface temperatures should be expected to vary about the average inlet temperature ($C_T = 1.0$) and not the temperature of the unheated inlet gas ($C_T = 0.0$), as in the case of the stator. Figure 7 clearly demonstrates this fact. In addition, there is a temperature peak on the pressure side at about 20% chord from the leading edge. This peak is about 40% higher than the average inlet C_T. This indicates that the local time-averaged temperatures on the rotor pressure side can be expected to be well in excess of the average inlet temperature. Over the next 60% of the chord the temperature is approximately equal to T_{av}. The pressure-side temperature then falls to 75% of $(C_T)_{av}$ at the trailing edge. The suction side shows a single maximum corresponding to a value of C_T 15% above $(C_T)_{av}$.

Figure 7 also shows the CO_2 concentrations obtained in the experimental study of Ref. 1. The CO_2 concentrations simulate surface temperatures. It can be seen that there is a rough qualitative agreement between the numerical and experimental temperature distributions. The pressure-side temperature peak is much higher and is located further downstream on the rotor pressure surface in the case of the experiment. The suction-side, experimental temperature distribution shows an extra temperature minimum and also drops to much lower values toward the trailing edge on the suction side.

Because the purpose of this study was to explore the ability of the calculation to capture the dominant physics of a hot streak, no attempt was made to eliminate a number of significant differences between the experimental setup and the basic computational setup described in Ref. 6. These differences must be kept in mind when one is comparing experimental and numerical results. The most important differences are as follows:

1) The actual flow is three-dimensional in nature (having significant local radial flows), whereas the present calculation is only two-dimensional.

2) The experimental configuration has 22 stator airfoils and 28 rotor airfoils, whereas the calculation had 22 of each with an enlarged rotor airfoil.

3) In the experiment, the hot gas entered the system through only one stator passage. The periodicity boundary condition used in the calculation produces a hot streak in every stator passage, resulting in a much greater amount of hot gas entering the stage. Another factor that results in a greater fraction of hot gases entering the stage in the numerical study is the two-dimensionality of the calculation; in the experiment the hot gases exit through a circular pipe that exists over one-third of the spanwise dimension. The two-dimensionality of the calculation is roughly equivalent to hot gases being introduced across the entire span from hub to tip.

4) The hot streak intensity was much higher in the experiment. The hot streak temperature was twice the temperature of the rest of the inlet gases (the numerical results were obtained with a proportionality factor of 1.2). This difference could have been eliminated, but it would have required additional machine time.

5) The axial gap between the stator and rotor airfoils in the experiment was 65% of the average chord length, whereas the value used in this exploratory numerical study was 15%.

6) The value of the flow coefficient (u_∞/U) in the experiment was 0.68, whereas that used in the calculation was 0.78 (the lower coefficient corresponds to a 5-deg rotor positive incidence relative to the higher coefficient). The lower flow coefficient of the experiment should accentuate the hot streak accumulation on the rotor pressure side.

Each of these differences between the experimental and computational setups has been the focus of ongoing work. These results will be reported on at a future date. It is interesting to note that in spite of all these differences between the experiment and calculation, the main features, such as pressure-side accumulation of the hot gases, are in agreement in the two analyses.

The higher temperatures on the pressure side of the rotor are a result of the accumulation of hot gases. Instead of averaging out the inlet temperature distortion, the rotor tends to segregate the heated and unheated inlet gases. This tendency of the rotor to segregate the hot and cold gases can be explained using the model of Ref. 5. The absolute velocity of the gas in the hot streak is higher than the average absolute velocity [Eqs. (5)]. In the rotor frame of reference, higher absolute rotor inlet velocities result in flow with not only a positive incidence relative to the rotor but also a flow with a higher relative total pressure. This results in a migration of the hot gases from the suction side of the rotor passage toward the pressure side, which in turn results in an accumulation of hot gas on the pressure side of the rotor airfoils.

Unsteady Temperatures

The temperature fluctuations on the stator are minimal because the hot streak does not directly impact the stator surface. However, the rotor surface temperatures exhibit significant temporal variations because of the passing of the rotor airfoil through the hot streaks. Figure 8 shows the magnitude of the temporal temperature fluctuation $\bar{C}_T$ along the surface of the rotor (plotted as a function of the arc length along the rotor). The quantity $\bar{C}_T$ is defined as

$$\bar{C}_T = \frac{T_{max} - T_{min}}{T_{hs} - T_\infty}$$

where T_{max} and T_{min} are the maximum and minimum temperatures that occur over a cycle at a given point.

The suction side of the rotor shows temporal temperature variations almost as large as the spatial temperature variations at the inlet of the stator. In other words, the rotor suction surface temperature varies from almost the inlet hot gas temperature to the inlet cold gas temperature in one cycle. This variation can be seen more clearly in Fig. 9, where the two components T_{min} and T_{max}, which constitute the amplitude curve of Fig. 8, are plotted. The minimum temperature is seen to be close to the inlet cold gas temperature. The pressure side of the rotor shows much smaller variations of temperature over the cycle. The minimum variation occurs close to the location where the pressure-side temperature peak occurs. An interesting feature of Fig. 9 is that the maximum temperature on the pressure side of the rotor is almost everywhere smaller

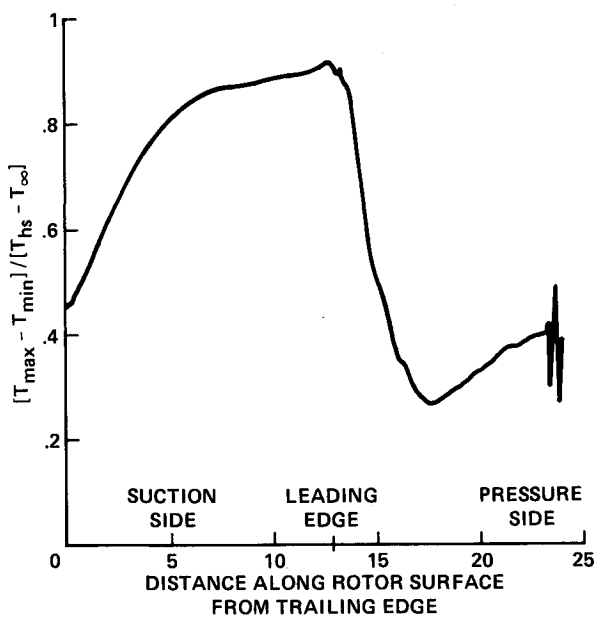

Fig. 8 Temperature amplitude distribution on the rotor.

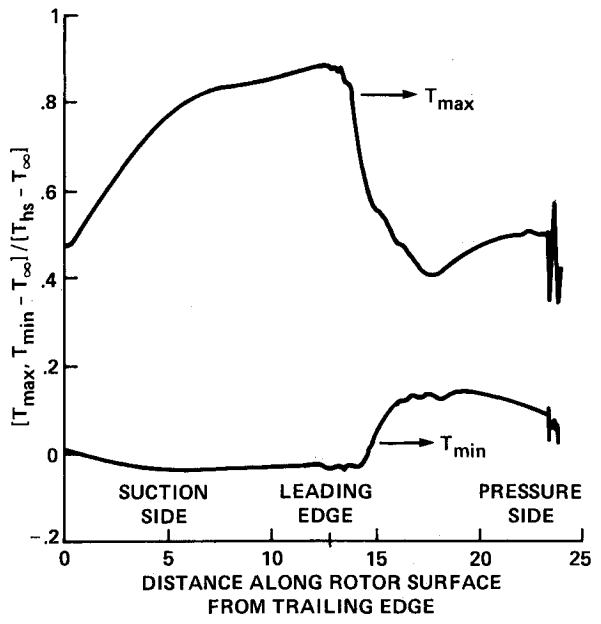

Fig. 9 Distribution of minimum and maximum temperatures on the rotor.

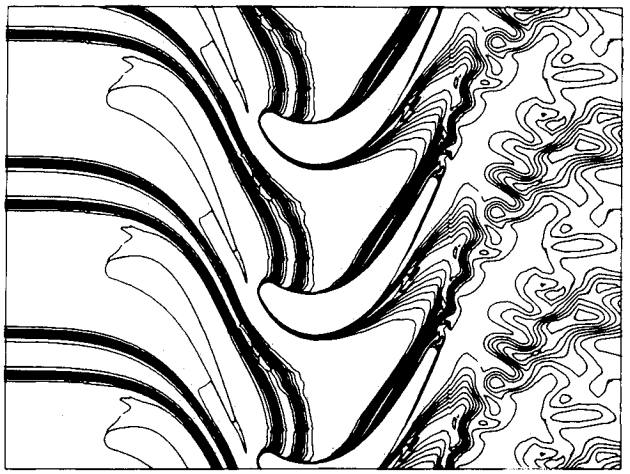

Fig. 10 Temperature contours ($t = 0.25$).

than the maximum temperature on the suction side. This indicates that the large suction-side maximum temperature exists for only a small portion of the cycle, because otherwise the time-averaged temperatures on the suction side would be much larger than those on the pressure side (see Fig. 7).

Temperature Contours

As mentioned earlier, one of the advantages of the computational approach is that it yields, as a part of the calculation, not only surface temperatures but also the temperature distribution in the entire region of interest. Figures 10–13 show the general behavior of the hot streak as it is convected through the turbine stage in terms of temperature contours in the stage at various positions in time (or different rotor-stator orientations). In Fig. 10 we see the hot streak entering the stator row from the left. The two bands of contours represent the areas where the temperature makes the transition from the hot gas temperature to the cold gas temperature. The narrow area in between these two bands constitutes the hot streak.

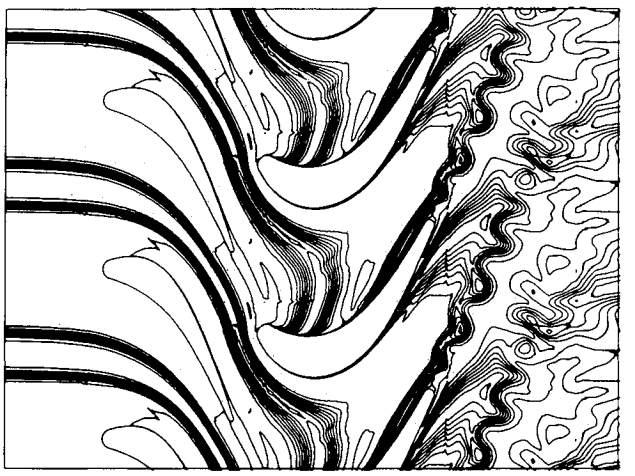

Fig. 11 Temperature contours ($t = 0.50$).

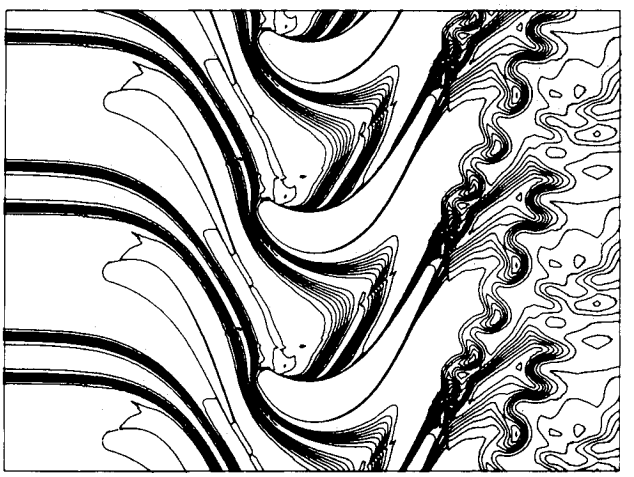

Fig. 12 Temperature contours ($t = 0.75$).

Since the static and absolute total pressures in the hot streak are the same as in the cold gas, the only redistribution mechanism in the stator row is a diffusion mechanism that is very weak. This results in the hot streak remaining intact in the stator row. The width of the hot streak decreases from the leading edge to the trailing edge because the flow is accelerating (a simple continuity argument explains the decrease in hot streak width).

A considerable redistribution of the inlet temperature distortion occurs when the hot streak enters the rotor row because the rotor passes through the hot streak as the rotor moves downward. Figure 10 shows the hot streak impinging close to the leading edge on the pressure side of the rotor. The downward motion of the hot gas upon entering the rotor row is clearly seen. The hot streak wraps itself around the rotor airfoil as it moves downstream. This results in the hot streak assuming the shape of a V during its travel through the rotor passage. Figure 10 also shows the V of the hot streak from the previous cycle as it exits from the rotor row.

The trailing edge of the rotor is quite blunt and consequently sheds vortices at a frequency quite different from the blade-passing frequency. The hot gas that is in and near the rotor boundary layer acts as a dye and graphically illustrates the shedding of vortices and the unsteady wake associated with the rotor airfoil. The shedding frequency was found to be approximately seven times the blade-passing frequency. The Strouhal number was estimated to be about 0.22 (this was

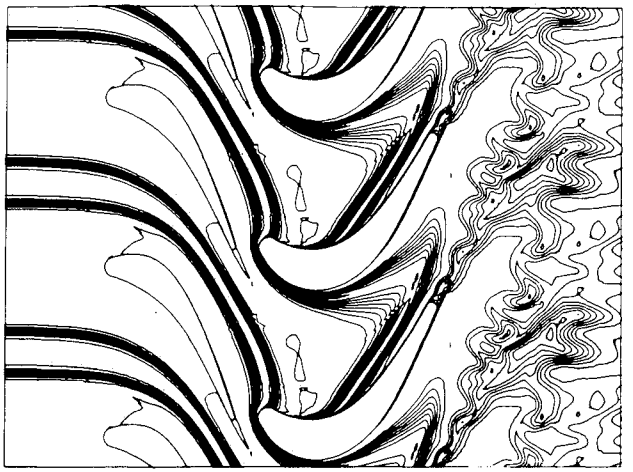

Fig. 13 Temperature contours ($t = 1.00$).

accomplished by taking the ratio of the diameter of the trailing-edge circle of the rotor and the distance between successive vortices. Reference 12 predicts a value of 0.21 for cylinders at Reynolds numbers between 1000 and 5000. The present calculation has an exit Reynolds number based on the diameter of the rotor trailing-edge circle of 35,000.

Figures 11–13 show temperature contours at various positions of the rotor with respect to the stator. Figure 11 shows the hot streak beginning to form a V. In Fig. 12 the V is distinct. This particular figure shows the vortex-shedding phenomenon clearly. Figure 13 shows a mixing of the hot gases associated with wakes of consecutive rotor airfoils.

Conclusions

This study uses an existing unsteady, two-dimensional, Navier-Stokes computer program to simulate the flow through a turbine stage. The program was easily modified to incorporate a hot streak in the inlet condition and was then used to simulate the redistribution of the inlet temperature distortion within the stage. The ease with which the necessary code changes were made and the short amount of time required to obtain a converged solution indicated that computational tools such as the one used in this study can be used to great advantage in understanding fluid mechanical phenomena in turbomachinery and the subsequent redesigning of such systems.

The results of the simulation indicated that the stator flowfield is, as expected, unaffected by the hot streak. This is because the total and static pressures in the hot streak were the same as in the rest of the inlet fluid, and also because the hot streak does not directly impact the stator airfoils. The rotor flowfield is altered significantly because the rotor airfoils pass through the hot streak. It was found that the hot gas migrated toward the pressure side of the rotor, creating a local hot spot on the pressure side. The rotor, instead of averaging out the nonuniformities in the inlet temperature, reacts to these nonuniformities.

A comparison of time-averaged, rotor-surface temperatures with experimental data showed a rough qualitative agreement between the two sets of data. It is believed that much better comparisons can be obtained by performing a three-dimensional calculation in which the geometry and inlet flow conditions are closer to the experimental values.

References

[1]Bulter, T. L., Sharma, O. P., Joslyn, H. D., and Dring, R. P., "Redistribution of an Inlet Temperature Distortion in an Axial Flow Turbine Stage," AIAA Paper 86-1468, June 1986.

[2]Munk, M., and Prim, R. C., "On the Multiplicity of Steady Gas Flows Having the Same Streamline Pattern," *Proceedings of the National Academy of Sciences,* Vol. 33, 1947.

[3]Hawthorne, W. R., "Secondary Vorticity in Stratified Compressible Fluids in Rotating Systems," Univ. of Cambridge, Cambridge, UK, Dept. of Engineering Rept. CUED/A-Turbo/TR 63, 1974.

[4]Lakshminarayana, B., "Effects of Inlet Temperature Gradients on Turbomachinery Performance," *ASME Journal of Engineering for Power*, Vol. 97, No. 1, Jan. 1975, pp. 64–74.

[5]Kerrebrock, J. L., and Mikoljczak, A. A., "Intra-Stator Transport of Rotor Wakes and its Effect on Compressor Performance," *ASME Journal of Engineering for Power,* Vol. 92, No. 4, Oct. 1970, pp. 359–368.

[6]Rai, M. M., "Navier-Stokes Simulations of Rotor-Interaction Using Patched and Overlaid Grids," *Journal of Propulsion and Power,* Vol. 3, No. 5, Sept. 1987, pp. 387–396.

[7]Rai, M. M., and Chakravarthy, S. R., "An Implicit Form of the Osher Upwind Scheme," *Journal of Propulsion and Power*, Vol. 24, No. 5, May 1986, pp. 735–743.

[8]Baldwin, B. S., and Lomax, H., "Thin Layer Approximation and Algebraic Model for Separated Turbulent Flow," AIAA Paper 78-257, Jan. 1978.

[9]Dring, R. P., Joslyn, H. D., Hardin, L. W., and Wagner, J. H., "Turbine Rotor-Stator Interaction," *Journal of Engineering for Power,* Vol. 104, Oct. 1982.

[10]Rai, M. M., and Chaussee, D. S., "New Implicit Boundary Procedures: Theory and Application," *AIAA Journal,* Vol. 22, No. 8, Aug. 1984, pp. 1094–1100.

[11]Rai, M. M., "Three-Dimensional Navier-Stokes Simulations of Turbine Rotor-Stator Interaction, Part 2—Results," *Journal of Propulsion and Power,* Vol. 5, No. 3, May–June 1989, pp. 312–319.

[12]Schlichting, H., *Boundary Layer Theory*, 6th ed., McGraw-Hill, New York, 1968, pp. 27–34.